Hydrocarbons on sea water: steady-state spreading signatures determined by an optical method*

OCEANOLOGIA, 49 (3), 2007.
pp. 413–437.

KEYWORDS
Liquid wettability
Crude oil derivatives
Oil pollution geometry
Optical method
Contamination
Assessment relations

Katarzyna Boniewicz-Szmyt[1]
Stanisław Pogorzelski[2]
Adriana Mazurek[2]

[1] Department of Physics,
Gdynia Maritime University,
Morska 81–87, PL–81–225 Gdynia, Poland;

e-mail: kbon@am.gdynia.pl

[2] Institute of Experimental Physics,
University of Gdańsk,
Wita Stwosza 57, PL–80–952 Gdańsk, Poland;

e-mail: fizsp@univ.gda.pl

Received 31 July 2006, revised 16 June 2007, accepted 29 June 2007.

Abstract

The spreading properties of several hydrocarbons (vegetable, engine, gear and crude oils) on distilled and artificial sea water were determined under laboratory conditions using a novel optical method. With the aid of Langmuir's equation, the geometrical signatures of a discrete lens of each hydrocarbon droplet floating on a water tank served to calculate the entering E (31.30–94.18 mN m^{-1}) and spreading S (-3.50 to -57.49 mN m^{-1}) coefficients, and equilibrium thicknesses t_∞ (0.20–1.25 cm). They appeared to be in agreement with the values derived

* The study was supported by grant BW/5200-5-0214-6 from the Polish Council for Scientific Research (KBN) and carried out in part within the framework of the scientific activity of the University of Gdańsk (supported from DS/5200-4-0024-06).

from direct interfacial tension measurements (Wilhelmy plate and stalagmometer methods). Empirical relations of the normalized lens radius r_L/r_{drop} and S on the water surface tension γ_{AW} were postulated as being of significant value in oil spill assessment studies at sea. The parameters obtained together with the surface properties of a natural surfactant-containing water body represent the principal input data required for modelling the spreading of a surface-tension-gradient-driven oil spill at sea.

1. Introduction

Both natural and pollutant (including oil discharge) films modify the physics and chemistry of the sea surface in ways detectable by various remote sensing systems (Clark 1993). At present, it is not possible to determine the location, extent, thickness and type of oil pollutant using just one single sensor system. The hypothesis presented here could lead to a practical, optical surveillance system for polluted sea areas applicable (after technical modifications) for continuous in situ monitoring of the inherent spreading signatures of oil spills at sea. Moreover, such surface spreading properties constitute the requisite input data for modelling the kinetics of oil spill spreading (Sebastião & Guedes Soares 2006). Whereas, in general, the spreading of large oil masses is driven chiefly by gravity, the morphology of the slick near its leading edge and over the entire covered area in the terminal stages of spreading is strongly affected by surface tension forces (Camp & Berg 1987). The surface properties (in particular, surface and interfacial tensions) of the water body itself are of key importance. Such information is crucial for determining actual or potential pollution pathways. The microlayer surfactants present in sea water (unlike artificial sea water) originate from several sources – petroleum, biological activity of plankton, terrestrial material or atmospheric precipitation (Hunter & Liss 1981) – and can affect the way oil spreads on water. In addition, the presence of surfactants in both the aqueous and oil (Bauget et al. 2001) phases can lead to interfacial tension gradients giving rise to Marangoni stresses that could also initiate and drive the spreading process (Craster & Matar 2006).

An understanding of the structure of liquids adjacent to other surfaces, and of how surface wettability is governed by interfacial forces or phenomena, is important in many technological, industrial, chemical and biological situations (Adamson & Gast 1997). In this paper we review recent experimental progress, provide a conceptual framework within which the majority of the spreading experiments can be understood and evaluated, and point out discrepancies between experiment and theory.

Oil entering and spreading at an air/water interface is of practical relevance to a wide range of industrial applications, from antifoaming action to the structural evaluation of crude oil spills at sea in oceanographic

studies. Once a droplet has entered the air/water interface, spreading may occur (Law 2001). The driving force for oil spreading is the balance of interfacial tensions γ at the air (A) – water (W) – oil (O) phase boundary. Complete wetting of the air/water interface by oil takes place when the spreading coefficient, $S = \gamma_{AW} - \gamma_{OW} - \gamma_{OA}$, is zero or positive, partial wetting when S is negative (Robinson & Woods 1948). Many food-grade and vegetable oils have $S < 0$ on clean water, whereas the less polar higher alkanes and crude oil derivatives often have $S < 0$ (Hotrum et al. 2005). In the latter case, the oil forms a lens of a particular equilibrium thickness t_∞ and is said to partially wet the air/water interface. However, what is still needed is a better understanding of the surface activity of asphaltenes and resins – the main surface-active components of crude oil affecting the interfacial tension γ_{AW} and γ_{OW} (Bauget et al. 2001). In the presence of an adsorbed surface-active film at the water surface, as often observed in polluted natural waters, γ_{AW} may be lowered sufficiently to bring S to negative values (Hotrum et al. 2002). It is important to note that the wetting transition refers exclusively to the initiation of the lens-to-uniform oil layer structural transition and coincides with the threshold γ_{AW} required for $S = 0$. The entering and spreading of oil droplets at quiescent air/water interfaces was studied in a water tank, where an optical method was adopted to assess the geometry of the lens shape. The thickness of a discrete lens of each hydrocarbon sample floating on a stagnant water pool was measured and used to calculate the spreading coefficient of the hydrocarbon, since the magnitude of S is proportional to the square of the thickness according to Langmuir's capillarity theory (Takii & Mori 1993, Akatsuka et al. 1995, Adamson & Gast 1997).

Generally, the magnitude of S is much smaller than the surface and interfacial tensions; hence, reasonable accuracy was not really expected in calculating S, as derived here from supplementary direct interfacial tension evaluations of γ_{AW}, γ_{OA} and γ_{OW} (stalagmometer-drop method), for comparison. The aim of the laboratory experiments was threefold. The entering and spreading properties of several hydrocarbons (vegetable, paraffin, olive, sunflower, engine and gear oils, pure higher alkanes and crude oils) on distilled water, as well as artificial and natural sea water were examined. A functional dependence of the normalized lens radius r_L/r_{drop} and S on γ_{AW} was obtained from the geometrical signatures of photographed lenses (thickness, radius and interfacial contact angles) over a wide range of γ_{AW} (varied by dissolving a surface active agent in the aqueous phase) starting from the threshold value. Finally, the spreading coefficients determined from the measurement of a circular, large-diameter

lens of uniform thickness and from the theoretically predicted equation for an infinitely large lens were compared to the data obtained from direct interfacial tension measurements. The temperature and lens-aging effects on the spreading properties of a wide group of crude oil derivatives on natural waters remain to be explored in further field studies.

2. Theoretical background

Thermodynamically, three conformations may arise for an oil droplet at an air/water interface. Robinson & Woods (1948) derived an entering coefficient E which predicts whether a droplet will enter the air/water interface or remain submerged in the water phase. It is given by

$$E = \gamma_{\mathrm{AW}} + \gamma_{\mathrm{OW}} + \gamma_{\mathrm{OA}}, \tag{1}$$

where γ is the interfacial tension, and the subscripts W, A, and O refer to water, air and oil, respectively. The entering of an oil droplet occurs when $E > 0$. It is important to understand that entering is the precursor to spreading. In the classical spreading theory, entering is predicted from equilibrium thermodynamics (Robinson & Woods 1948). Moreover, it has been shown that entering is influenced by the kinetic aspect of the rupturing of the thin film separating the oil droplet from the air/water interface (Bergeron et al. 1993, Lobo & Wasan 1993). Owing to their coherent nature, protein films can effectively inhibit droplet entering by lending mechanical stability to the thin film (Hotrum et al. 2002, Hotrum et al. 2003). Once entered, a droplet may either form a lens or spread out into a film covering the air/water interface.

The tendency of an oil droplet to spread at an air/water interface is predicted by the spreading coefficient S defined by Harkins & Feldman (1922) as

$$S = \gamma_{\mathrm{AW}} - \gamma_{\mathrm{OW}} - \gamma_{\mathrm{OA}}. \tag{2}$$

When S is positive, oil spreads. Triglyceride oils with medium to long-chain fatty acids, such as soybean, or liquid butter oil, have $S > 0$, and can, therefore, spread at a clean air/water interface (Harkins & Feldman 1922, Schokker et al. 2002, Hotrum et al. 2004, 2005). Oil spreading is inhibited if γ_{AW} (= the threshold value) becomes so low that the condition $\gamma_{\mathrm{AW}} > \gamma_{\mathrm{OW}} + \gamma_{\mathrm{OA}}$ is no longer satisfied, for example, due to the presence of an adsorbed protein layer (Harkins & Feldman 1922).

However, the three conformations can be predicted based on the balance of interfacial tensions for the initial system (i.e. before the oil droplet comes into contact with the air/water interface): they are $E < 0$, $S < 0 < E$, and $S > 0$, respectively. When $E < 0$ the droplet remains wetted by the aqueous phase and submerged under the air/water interface. For the condition

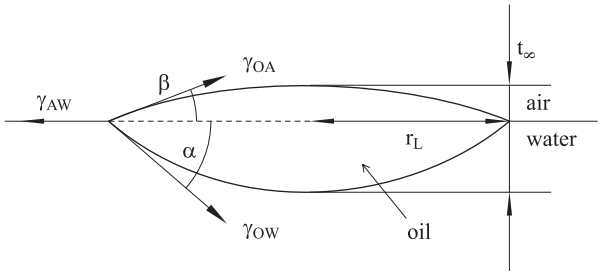

Fig. 1. A stationary oil lens on an air/water interface showing the relevant interfacial tensions and contact angles (α and β); γ is the surface tension and the subscripts A, O, and W refer to air, oil, and water, respectively; t_∞ is the equilibrium lens thickness

$S < 0 < E$, the oil droplet enters the air/water interface and forms a lens. The radius of the lens increases with increasing γ_{AW} until the condition $S = 0$ is reached. When $S > 0$ a spread oil film will be formed replacing the air/water interface with an oil/water interface (see Fig. 1 in Hotrum et al. (2002)).

For a stationary oil lens at the air/water interface, the contact angles α and β, the relevant interfacial tensions and its geometric signatures (lens radius r_L and equilibrium thickness t_∞) are shown diagrammatically in Figure 1.

The assumptions that gravitational effects and line tension could be neglected were made in the calculation of the lens radius r_L. They are satisfied when the periphery of the surface is at a distance from the lens periphery of more than several times the capillary length $L_C = (2\gamma_{AW}/\rho_W g)^{1/2}$, where ρ_W is the mass density of water, and g the acceleration due to gravity.

Resolving the Neumann triangle of interfacial forces (Fig. 1) horizontally at the three-phase contact line yields

$$\gamma_{AW} = \gamma_{OW}\cos\alpha + \gamma_{OA}\cos\beta. \tag{3}$$

From eq. (3) it follows that the angles α and β are given by (Pujado & Scriven 1972, Retter & Vollhardt 1993, Aveyard & Clint 1997)

$$\cos\alpha = \frac{\gamma_{AW}^2 + \gamma_{OW}^2 - \gamma_{OA}^2}{2\gamma_{OW}\gamma_{WA}}, \tag{4}$$

$$\cos\beta = \frac{\gamma_{AW}^2 + \gamma_{OA}^2 - \gamma_{OW}^2}{2\gamma_{OA}\gamma_{WA}}. \tag{5}$$

The total volume of the drop before entering $V_{drop} = 4\pi r_{drop}^3/3 = V_1 + V_2$, where V_1 and V_2 are the respective volumes of the upper and

lower lens caps (depicted in Fig. 1). From geometry, V_1 and V_2 are given by (Retter & Vollhardt 1993, Aveyard & Clint 1997)

$$V_1 = \frac{\pi r_L^3}{3\sin^3\beta}(\cos^3\beta - 3\cos\beta + 2), \tag{6}$$

$$V_2 = \frac{\pi r_L^3}{3\sin^3\alpha}(\cos^3\alpha - 3\cos\alpha + 2). \tag{7}$$

Thus, when V_{drop} and the respective interfacial tensions are known, r_L can be calculated and referred to the drop radius r_{drop} to obtain the normalized lens radius r_L/r_{drop}.

Any hydrocarbon with negative S and a density lower than that of water relaxes to form a circular, biconvex lens if it is fed onto a water surface at a fixed location far from the periphery of the surface, such that it is practically independent of either the geometry of the periphery itself or the water meniscus possibly forming at the periphery.

The major difficulty in determining the values of S lies in the fact that their magnitudes are much smaller than those of the surface and the interfacial tensions. Thus, S can never be determined with sufficient confidence from individual experimental data on γ_{AW}, γ_{OA} and γ_{OW} (Takii & Mori 1993).

The recommended method for determining S is to measure the almost uniform thickness, t_∞, of a circular, large-diameter lens of a hydrocarbon liquid floating on the surface of a quiescent water pool and then to calculate S with the aid of Langmuir's force-balance equation for an infinitely large lens (Adamson & Gast 1997)

$$S = -\frac{1}{2}\left(1 - \frac{\rho_O}{\rho_W}\right)\rho_O g t_\infty^2, \tag{8}$$

where ρ_O denotes the mass density of the hydrocarbon, and t_∞ is the thickness of an infinitely large lens. For many hydrocarbons, the spreading coefficient is found to increase asymptotically towards zero with increasing temperature (Akatsuka et al. 1995).

3. Experimental methodology

3.1. Materials

Twice-distilled water and artificial sea water were used as the substrates for the hydrocarbon lenses. Artificial sea water was prepared as a solution of 0.56 M NaCl, 0.05 M $MgSO_4 \times 7\,H_2O$ and 0.01 M $CaCl_2 \times H_2O$. The pH of the solution was adjusted to pH 8.4 by the addition of 0.1 M HCl or NaOH. Natural sea water samples were collected in shallow coastal waters of the

Baltic Sea. The sampling site locations are shown in Figure 1 in Pogorzelski & Kogut (2003). The hydrocarbons used in the model studies represent different classes of crude oil products: engine and gear oils, original crude oils (Russian, Baltic and Flotta) and vegetable oils (sunflower, olive, paraffin oils). All the oils were used as received without any prior physicochemical treatment.

In order to change the surface tension of the aqueous sub-phase γ_{AW}, a certain quantity of wetting agent (Fotonal (trade name), used in photography) was dissolved. The decrease in surface tension $\Delta\gamma_{AW}$ (surface pressure Π_{AW}) was related to the bulk concentration of the substance c via Szyszkowski's empirical equation (Adamson & Gast 1997): $\Pi_{AW} \equiv \gamma_{AW} = RT\Gamma_\infty \ln(1 + c/a)$, where Γ_∞ is the saturation adsorption ($\Gamma_\infty = 2{\times}10^{-10}$ mol cm^{-2}), Szyszkowski's surface activity coefficient a = 10^{-6} mol cm^{-3}, R is the gas constant and T the absolute temperature (K). Fotonal suppresses γ_{AW} to low values of 32.8 mN m^{-1} at the critical saturation concentration (cmc $-$ c$_\infty$ = 0.0145 vol. %).

3.2. Apparatus and procedure

The experimental apparatus used in laboratory studies of hydrocarbon wetting on water surface is shown diagrammatically in Figure 2.

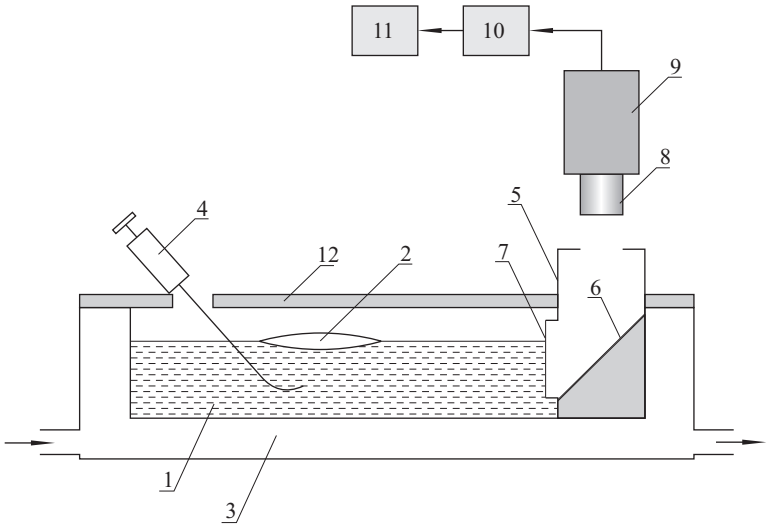

Fig. 2. The experimental set-up (cross-sectional side view); 1 – water tank, 2 – hydrocarbon lens, 3 – double-walled thermostatted water bath, 4 – hydrocarbon dosing syringe, 5 – periscope tube, 6 – inclined mirror, 7 – foil-covered window, 8 – objective, 9 – black/white CCD camera, 10 – frame grabber USB unit, 11 – PC-class computer, 12 – water pool roof, → thermostatted water flow

A hydrocarbon drop was produced at the tip of the U-shaped needle using a microsyringe (4) and released into the water pool – a rectangular ($30 \times 40 \times 5$ cm), plastic tank (1). The drop rose to the surface of the tank and resolved itself into a floating biconvex lens (2).

Each experiment was started by the supply of a small amount (3–8 cm^3) of hydrocarbon to the surface of the water to form a single lens, 75–110 mm in diameter; this is large enough for it to have flat surfaces over its central part, but not so large as to interact with the water meniscus at the edge of the container.

The aqueous sub-phase was temperature-controlled with an accuracy of ± 0.2 K using a thermostatted water circulation system through the tank walls (3). After the elapse of some 15 min to permit the water and hydrocarbon phases in the test area to reach uniform temperature, the drop, which appeared to have turned into a stable lens (2), was photographed repeatedly through the window (with a transparent net scale) in a periscope system (7) with an optical lens – a CCD camera system (magnification $\times 15$) (8, 9). The outer side (in contact with water) of the periscope was covered with a polyolefin foil (providing a foil/water contact angle of 90° in order to eliminate the meniscus, thus allowing the lens to be photographed in an undisturbed state. The geometrical signatures (interfacial contact angles, lens radius and equilibrium thickness) of each lens were determined from digital photo processing using a PC and frame grabber unit (10, 11).

In order to characterize the hydrocarbon materials, the following physical parameters were measured: density (volumetrically), surface and interfacial tensions in contact with the aqueous phase (using the Wilhelmy plate and stalagmometer-drop methods (Adamson & Gast 1997)).

The oil/water and oil/air interfacial tensions of the systems were measured at 1 s intervals using a filter paper (5 cm wide) and a roughened glass (20 mm $\times$ 20 mm $\times$ 1 mm) slide – the Wilhelmy plate sensors – suspended from a force transducer (GM2 + UL5, Scaime, France) and were accurate to within 0.1 mN m^{-1}. All measurements were performed at room temperature 22 ± 0.5°C.

4. Results and discussion

An example image of a sunflower oil drop lens of volume $V_{drop} = 0.2$ cm^3 floating on a water surface at T = 22°C is shown in Figure 3. This lens had a radius r_L and thicknesses t of 0.66 and 0.26 cm, respectively. The surface and interfacial tensions (γ_{OA} = 32.17 mN m^{-1}, γ_{OW} = 58.16 mN m^{-1}, γ_{AW} = 32.84 mN m^{-1}), the corresponding interfacial contact angles ($\alpha = 29.8°$, $\beta = 21.2°$) and $V_1 = 0.08$ and $V_2 = 0.12$ cm^3 were calculated from the lens geometry analysis by means of eqs. (4)–(7).

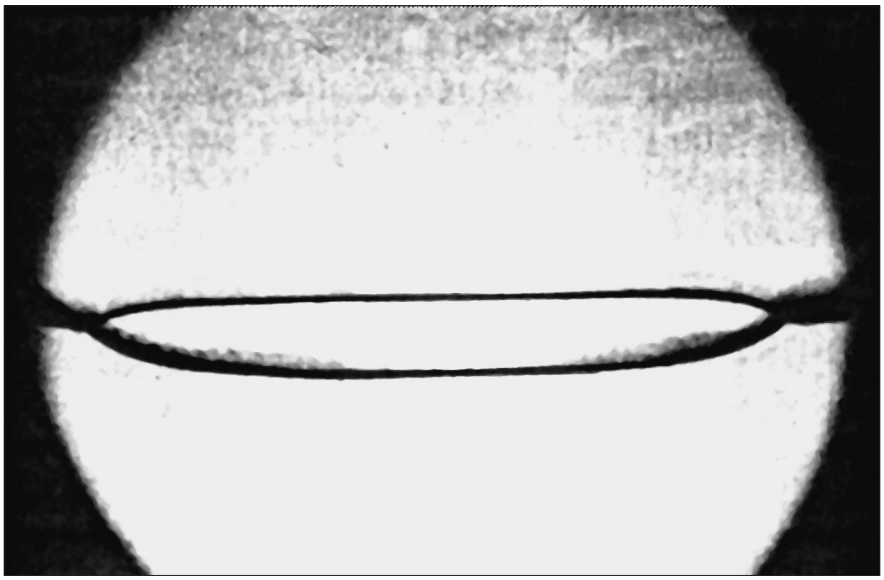

Fig. 3. A sunflower oil drop lens of volume $V_{drop} = 0.2$ cm^3 floating on a water surface at T = 22°C. The lens has a radius $r_L = 0.66$ cm and thickness t = 0.26 cm. The corresponding surface and interfacial tensions are $\gamma_{OA} = 32.17$ mN m^{-1}, $\gamma_{OW} = 58.16$ mN m^{-1}, $\gamma_{AW} = 32.84$ mN m^{-1} with contact angles at interfaces $\alpha = 29.8°$, $\beta = 21.2°$

The wettability parameters of the hydrocarbons examined in this study and those gleaned from the literature data on water surfaces together with the geometrical signatures of the oil lenses obtained with eqs. (4)–(7) are set out in Table 1.

The oil entered the surface in all the hydrocarbon-water systems considered here (E values positive, from 31.30 to 94.18 mN m^{-1}). The highest values were noted for rather heavy, viscous engine and gear oils and also for higher homologues of paraffin oils (e.g., n-hexadecane and n-decane). Generally, values of S were negative (from -3.5 to -57.49 mN m^{-1}), which suggests the ability to form on the water surface a lens of equilibrium thickness t_∞ from 0.20 to 1.25 cm and normalized radius $r_L/r_{drop} = 1.29 - 2.01$. However, there were two hydrocarbons (see 12 and 15 in Table 1) capable of forming uniform layers on the water surface (the complete spreading case) with thicknesses from monomolecular to unity, according to the amount of liquid and surface available. This effect may have been due to the presence of trace quantities of surface-active additives in the gas oils, giving rise to adsorbed surface films at the A/W and O/W interfaces thereby altering the values of S. It is interesting to compare the spreading behaviour of sunflower oil observed during this study and that

Table 1. The wettability parameters of hydrocarbons on water and the geometrical signatures of oil lenses at T = 22°

Hydrocarbon	ρ_O	γ_{OA}	γ_{OW}	E	S	t_∞	α	β	r_L/r_{drop}	Remarks
	[kg m^{-3}]	[mN m^{-1}]				[m] $\times 10^{-2}$	[°]		[–]	
gear oil-Marinol 111	889.21	29.00	46.99	50.83	−43.15	0.96	37.22	35.50	1.57	γ_{AW} = 32.84 mN m^{-1}
paraffin oil	876.72	29.27	50.30	54.08	−46.52	0.95	33.05	29.58	1.66	
vegetable oil	914.57	31.25	51.01	52.61	−49.41	1.15	36.08	30.07	1.63	
body-care oil	856.88	29.28	49.65	53.22	−46.09	0.88	34.11	24.65	1.70	
olive oil	916.27	31.80	53.91	54.96	−52.86	1.21	32.62	23.93	1.72	
sunflower oil	915.34	32.17	58.16	58.84	−57.49	1.25	26.17	21.75	1.83	
crude oil	920.50	35.15	46.52	83.73	−9.31	0.49	32.15	23.71	1.73	data from Kaniewski (1974)
engine oil-Extra 11, pure	854.40	35.27	48.36	86.15	−11.72	0.38	36.18	25.85	1.67	γ_{AW} = 72.35 mN m^{-1}
engine oil-Extra 11, used	898.60	33.27	46.42	85.51	−7.33	0.33	29.57	20.71	1.80	
gear oil-Marinol 116, pure	853.00	36.85	51.54	88.20	−16.03	0.46	42.43	28.84	1.58	
gear oil-Marinol 116, used	872.00	34.25	48.72	86.83	−10.61	0.38	35.51	24.10	1.69	
diesel oil L-2	847.30	30.61	29.20	70.95	12.55					
gear oil-Melina 30, Shell, pure	897.70	35.85	50.60	87.11	−14.09	0.48	40.25	27.24	1.61	
gear oil-Melina 30, shell, used	905.20	34.12	49.05	87.29	−10.81	0.43	36.02	24.15	1.68	

Table 1. (*continued*)

Hydrocarbon	ρ_O	γ_{OA}	γ_{OW}	E	S	t_∞	α	β	r_L/r_{drop}	Remarks
	[kg m^{-3}]	[mN m^{-1}]				[m] $\times 10^{-2}$	[°]		[–]	
decane ($C_{10}H_{12}$)	730.00	23.90	45.48	94.18	3.22					data from Adamson & Gast (1997)
hexadecane ($C_{16}H_{34}$)	775.00	27.64	48.47	93.43	−3.51	0.20	23.33	13.05	2.01	$\gamma_{AW} = 72.60$ mN m^{-1}
sunflower oil	920.00	28.00	29.30	31.30	−27.30	0.86	60.60	56.36	1.29	data from Hortum et al. (2003)
n-tetradecane	782.00	26.00	47.00	51.00	−43.00	0.71	30.39	24.00	1.75	$\gamma_{AW} = 30.00$ mN m^{-1}

Symbols: ρ_O – oil density; γ_{OA} – oil/air interfacial tension; γ_{OW} – oil/water interfacial tension; *E, S* – entering and spreading coefficients; t_∞ – equilibrium lens thickness; α, β – interfacial air/water/oil contact angles; r_L/r_{drop} – relative oil lens radius.

reported by others (see 6 and 17 in Table 1). A similar lowering of surface tension (γ_{AW} = 32.84 and 30.00 mN m^{-1}), achieved by the addition of a certain amount of surface active agent to distilled water, leads to a significant change in γ_{OW}(= 58.16 and 29.30 mN m^{-1}, respectively), leaving γ_{OA} almost unchanged (= 32.17 and 28.00 mN m^{-1}). This suggests that the surface adsorption effect at the O/W interface is dependent on the elastic properties of the film (not controlled in these studies) (Bergeron et al. 1993, Lobo & Wasan 1993).

In order to test the sensitivity, accuracy and practical aspects of a novel optical method for determining hydrocarbon wettability on water, spreading parameters were compared using direct measurements of interfacial tension on the same oil-water systems. The mean wettability parameters (averaged over 4–6 measuring runs) and geometrical signatures of an oil drop lens are listed in Table 2. The interfacial tension γ_{OW} differed between the two data sets by several dozen percent, but γ_{OA} varied only within a few percent. Values of S were very different for heavy gear and vegetable (food grade) oils, but were comparable for the remaining oils. The entering coefficient was positive for all the systems studied but with a significant variability of the order of 20–30%. As a consequence of the differences in interfacial tension, there were certain discrepancies in the lens geometry parameters.

The equilibrium thicknesses were the same within the measurement accuracy for light body-care, olive and sunflower oils, but differed by several dozen per cent for the heavier gear, paraffin and vegetable oils. In contrast, the values of r_L/r_{drop} were in excellent agreement (within 2–7%; see 1–3 and 7–9 in Table 2) for the heavier hydrocarbons, but differed by 11–19% for the lighter ones. There are several possible sources of the discrepancies between the wettability signatures of these oil-water systems obtained by the two methods. The S values entering the theoretical equations for r_L/r_{drop} and t_∞ are assumed to be the equilibrium (or final) spreading coefficient data, where the surface and interfacial tensions of water and a hydrocarbon each saturated with the other and in contact with a gaseous phase are assumed. In the floating oil lens method, the image of the shape is recorded 10–15 minutes following the deposition of the hydrocarbon. On the other hand, in the stalagmometric interfacial tension measurements, the liquid drop is formed within a few seconds; this could result in an interfacial system state very far from equilibrium. In addition, a significant part may be played by surface dilation viscoelasticity: this gives some indication of the rigidity of the adsorptive film formed at the A/W and O/W interfaces (not controlled here), which, in turn, are dependent on the kinetics of interface formation. In general, a liquid hydrocarbon placed on the water surface formed

Table 2. Comparison of the wettability coefficients derived from optical (based on lens geometry) and direct interfacial tension measurements (stalagmometer and Wilhelmy plate methods) for a constant value of $\gamma_{AW} = 32.84$ mN m^{-1} at T = 22°C

Hydrocarbon	ρ_O	γ_{OA}	γ_{OW}	E	S	t_∞	α	β	r_L/r_{drop}	Remarks
	[kg m^{-3}]	[mN m^{-1}]				[m] $\times 10^{-2}$	[°]		[–]	
gear oil- Marinol 111	889.21	29.00	46.99	50.83	−43.15	0.96	37.22	35.50	1.57	optical method
paraffin oil	876.72	29.07	50.30	54.08	−46.52	0.95	33.05	29.58	1.66	
vegetable oil	914.57	31.25	51.01	52.61	−49.41	1.15	36.08	30.07	1.63	
body-care oil	856.88	29.28	49.65	53.22	−46.09	0.88	34.11	24.65	1.70	
olive oil	916.27	31.80	53.91	54.96	−52.86	1.21	32.62	23.93	1.72	
sunflower oil	915.34	32.17	58.16	58.84	−57.49	1.25	26.17	21.75	1.83	
gear oil- Marinol 111	889.21	29.00	27.62	30.78	−24.46	0.72	43.90	23.68	1.61	direct stalagmometer method
paraffin oil	876.72	29.07	40.21	43.31	−37.12	0.85	41.98	25.27	1.61	
vegetable oil	914.57	31.25	49.31	70.74	−68.91	1.36	33.64	20.55	1.75	
body-care oil	856.88	29.28	42.07	44.95	−39.19	0.81	24.94	15.14	1.95	
olive oil	916.27	31.80	52.72	53.08	−52.35	1.20	23.67	21.77	1.87	
sunflower oil	915.34	32.17	57.30	57.30	−57.31	1.25	35.92	26.20	1.67	
crude oil Russia	848.01	25.76	83.17	89.57	−76.77	1.11	29.29	19.73	1.82	
crude oil Flotta	874.83	28.04	66.82	70.94	−62.69	1.09	39.66	19.48	1.69	
crude oil Baltic	806.88	25.74	78.46	84.88	−72.040.98	54.92	20.16	1.52		

Symbols: ρ_O – oil density; γ_{OA} – oil/air interfacial tension; γ_{OW} – oil/water interfacial tension; E, S – entering and spreading coefficients; t_∞ – equilibrium lens thickness; α, β – interfacial air/water/oil contact angles; r_L/r_{drop} – relative oil lens radius.

an exceedingly thin lens, and subsequently tended to contract, resulting in a sharp increase in thickness t. This behaviour may well be due to the adsorption of hydrocarbon molecules onto the water surface. This means that equilibrium is achieved after a certain period, since lens aging was observed (Takii & Mori 1993).

Figure 4 shows a diagrammatic representation of the wetting transition for the hydrocarbons studied. The spreading coefficient is shown as a function of γ_{AW} and $\Pi_{AW}(= \gamma^0_{AW} - \gamma_{AW})$, where γ^0_{AW} is the surface tension of a clean air/water interface = 72.22 mN m^{-1}, and γ_{AW} is the actual air/water surface tension (varied by adding a surface active agent to the water phase). When $S < 0$, the oil droplet partially wets the air/water interface forming a lens. But when $S = 0$, the wettability transition takes place and a spread oil layer completely covering the surface is formed. The vertical dashed line at γ^0_{AW} indicates the physically accessible upper limit for γ_{AW}.

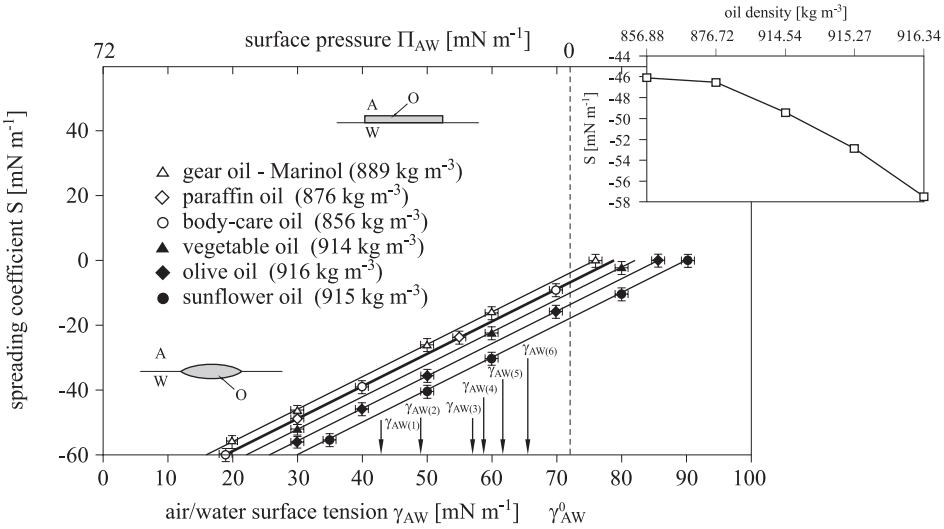

Fig. 4. Diagram showing the wetting transition for oils on water. The spreading coefficient S as a function of γ_{AW} and Π_{AW}, where the surface pressure $\Pi_{AW} = \gamma^0_{AW} - \gamma_{AW}$ was varied by adding a surface-active substance. Arrows indicate the surface tensions of natural water samples collected in the Gdańsk port channel (Wisłoujście) $\gamma_{AW}(1)$ and shallow coastal Baltic sea waters (Brzeźno) $\gamma_{AW}(2)$, (Jelitkowo) $\gamma_{AW}(3)$, (Orłowo) $\gamma_{AW}(4)$, (Gdynia) $\gamma_{AW}(5)$ and (Sopot) $\gamma_{AW}(6)$. The vertical dashed line corresponds to the upper limit for γ_{AW} = 72.2 mN m^{-1}. Inset: spreading coefficient versus density of the oil phase

Since the linear dependences $S(\gamma_{AW})$, the best-fit approximations to the experimental data, yield a threshold value of γ_{AW} ranging from 75

to 91 mN m^{-1} when extrapolated to $S = 0$, none of the oils can spread over the water surface. The arrows indicate that the surface tensions of the water samples collected in the Gdańsk port channel (Wisłoujście-1) and in Baltic coastal waters (Brzeźno-2), (Jelitkowo-3), (Orłowo-4), (Gdynia-5) and (Sopot-6) are significantly lower than γ^0_{AW}. We can write $S = \gamma_{AW} + B$, where the best-fit parameters A and B are set out in Table 3; this equation is useful for a rough estimate of S based on field measurements of the surface tension of water. A systematic relation between spreading coefficients and hydrocarbon density (given in brackets for each oil in Fig. 4) is evident ($S\uparrow$ as $\rho_O\downarrow$; see (Fig. 4 – inset). The smaller negative values of B in Table 3 are accompanied by greater oil densities. This tallies with the increase in surface tension γ_{AO} corresponding to the decreasing density of long-chain paraffin hydrocarbons. When V_{drop} and the respective interfacial tensions are known from the floating lens images, r_L can be calculated by means of eqs. (4)–(7).

The relative lens radius for three selected oil droplets deposited at the air/water interface vs. air/water surface tension are shown in Figure 5. Three possible conformations of an oil/water system, the corresponding inequalities for the entering and spreading coefficients with the vertical dashed border lines are also depicted. The curves in Figure 5 plunge to zero as E goes to 1 (in the range of realistic γ_{AW} values of sea water samples), indicating that when $E < 0$, the droplet remains wetted by the aqueous phase; nevertheless, the structural form of such an oil-water system is physically inaccessible to the oils studied here (see the values of E in Table 1). For the condition $S < 0 < E$, the oil droplet enters the air/water interface and forms a lens. The radius of the lens increases with increasing γ_{AW} until the condition $S = 0$ is reached. At this point the curve increases asymptotically to infinity. The asymptotic right-hand border lines occur at $\gamma_{AW} = 76.0$, 78.94 and 82.26 mN m^{-1}. When $S > 0$ (a situation not found here) a spread film will be formed covering all the available air/water surface.

In the presence of a surface-active material adsorbed at the A/W interface, the surface tensions may change as the oil spreads due to compression of the adsorbed layer by the expanding film (Hotrum et al. 2002). Spreading of the film may stop when the condition $S_e = 0$ is reached. The arrows point to the surface tensions of the natural water samples collected in the Gdańsk port channel (Wisłoujście $\gamma_{AW}(1)$) and Baltic sea coastal waters (Brzeźno-$\gamma_{AW}(2)$); (Jelitkowo-$\gamma_{AW}(3)$); (Orłowo-$\gamma_{AW}(4)$); (Gdynia-$\gamma_{AW}(5)$); (Sopot-$\gamma_{AW}(6)$), which are shown here for comparison. The experimental data can be quantitatively expressed by an exponential-

Table 3. Best-fit constants in the empirical relations of S and r_L/r_{drop} versus γ_{AW}, and S against r_L

Hydrocarbon	A [–]	B [mN m^{-1}]	R^2	C [–]	D [mN m^{-1}]	R^2	E [–]	F [mN m^{-1}]	R^2
gear oil-Marinol 111	1	−76.01 (3.56)	1	0.49 (0.03)	0.0003	0.96	−15.20 (0.76)	3.26 (0.16)	0.84
paraffin oil	1	−79.38 (4.01)	1	0.44 (0.02)	0.0002	0.94	−19.69 (0.98)	4.98 (0.24)	0.96
vegetable oil	1	−82.26 (4.52)	1	0.46 (0.02)	0.0002	0.97	−14.11 (0.70)	2.63 (0.13)	0.98
body-care oil	1	−78.94 (3.61)	1	0.37 (0.03)	0.0002	0.96	−18.99 (0.94)	4.17 (0.21)	0.99
olive oil	1	−85.72 (4.31)	1	0.39 (0.04)	0.0002	0.91	−12.75 (0.63)	2.47 (0.12)	0.98
sunflower oil	1	−90.34 (4.85)	1	0.34 (0.03)	0.0001	0.96	−11.52 (0.57)	2.14 (0.10)	0.97

Symbols: A, B – best-fit parameters in the relation: $S = A + B$; C, D – best-fit constants in the dependence $r_L/r_{drop} = C_{exp}(D\gamma_{AW}^2)$; E, F – best-fit coefficients in the relation $S = Er_L + F$; R – correlation coefficient. Standard deviations are given below the mean values (in brackets).

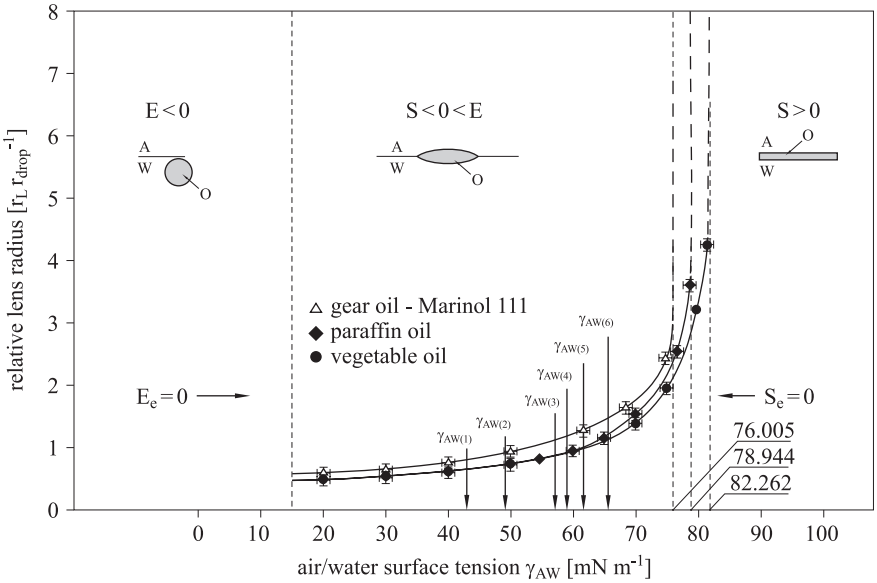

Fig. 5. Relative lens radius r_L/r_{drop} for three selected oil droplets floating on an air/water interface vs. air/water surface tension. Arrows indicate the surface tensions of water samples collected in the Gdańsk port channel (Wisłoujście) $\gamma_{AW}(1)$ and shallow coastal Baltic sea waters (Brzeźno) $\gamma_{AW}(2)$, (Jelitkowo) $\gamma_{AW}(3)$, (Orłowo) $\gamma_{AW}(4)$, (Gdynia) $\gamma_{AW}(5)$ and (Sopot) $\gamma_{AW}(6)$. The vertical dashed lines on the right correspond to the upper limit for γ_{AW}

power-law function – $r_L/r_{drop} = C\ \exp(D\gamma_{AW}^2)$ – the best-fit parameters C and D are listed in Table 3. For the first time, an important relation of the normalized relative lens radius on the water surface tension was obtained, which is of significant value in oil spill assessment techniques.

The spreading coefficient S as a function of the oil lens radius r_L obtained with an optical method for the oils is shown in Figure 6. Having measured the thickness of the lens, which has increased its volume until its surface becomes sufficiently flat over a substantial portion along its radius, one can calculate using eq. (8) the magnitude of S, which is proportional to the square of the equilibrium thickness. The values of t_∞ obtained for olive and vegetable oils are respectively equal to 1.21 and 1.15 cm, and correspond to the equilibrium lens radii $r_{L\infty}$ of 8.23 and 4.78 cm, related via eqs. (4)–(7) (see the vertical dashed lines in Fig. 6). Hence, the measured spreading coefficients $S = -52.86$ and -49.41 mN m^{-1} (see the horizontal dashed lines in Fig. 6) are in agreement with those predicted from eq. (8). Such an approach appears to be valid for sufficiently large lenses, where the interfacial tension forces can be neglected with respect to gravity (Adamson & Gast 1997). From a physical point of view, this condition can be met if

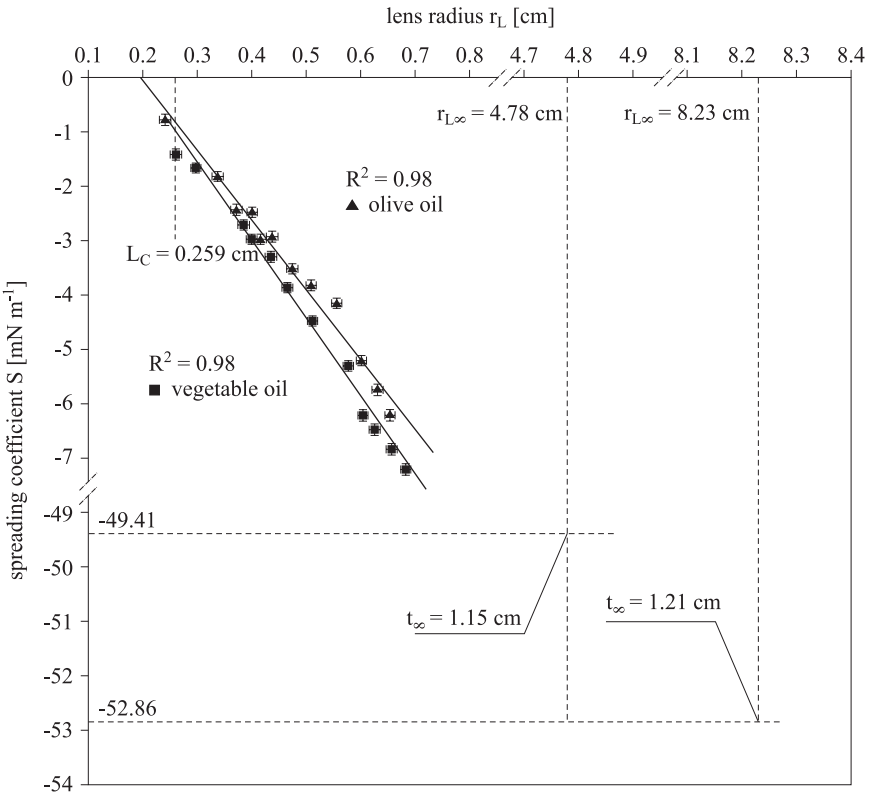

Fig. 6. The spreading coefficient S as a function of the oil lens radius r_L obtained with an optical method (based on the relation $S = -1/2(1 - \rho_O/\rho_W)\rho_O g t_\infty^2$). The solid lines are the best-fit linear approximations to the data points. The vertical dashed lines indicate the lens radii $r_{L\infty}$ corresponding to the infinitely large lens dimension case ($r_L \sim t_\infty$, for the particular spreading coefficients – given by the horizontal dashed lines of each oil). For comparison, the capillary length $L_C = (2\gamma_{AW}/\rho_W g)^{1/2}$ for water is also given

the lens is several times larger than the capillary length L_C (= 0.26 cm for pure water) (Law 2001). For small oil spots on water of radii < 1 cm, S is a quantity dependent on the lens dimension that becomes less negative as r_L decreases. As a first approximation, the empirical linear dependence between S and r_L can be postulated as $S = E\ r_L + F$, where the best-fit parameters E and F are given in Table 3 for all the hydrocarbons in the range 0.2 cm $< r_L <$ 3 cm. As Takii & Mori (1993) have already argued, substitution of each measured lens thickness t for t_∞, to which S is theoretically related (eq. (8)), leads to ever greater inaccuracy of such an approximation with increasing t. Experimental studies performed on n-decane, which forms the thickest lenses ($t \approx 1.6$ cm), have shown that the

excess of t over t_∞ is estimated to be $\sim 7\%$, and hence the substitution of t for t_∞ should result in the overestimation of $|S|$ by $\sim$14%.

The spreading properties of the hydrocarbons studied and the geometrical signatures of the layers formed were evaluated in terms of the surface tension of water γ_{AW}. The equilibrium air/water surface tension was controlled in this study by varying the concentration of a commercially available detergent (Fotonal); the relevant plot of $\gamma_{AW}(c)$ is shown in Figure 7a. The experimental dependence plotted against the concentration (vol. %) follows Szyszkowski's equation with the parameters $\Gamma_\infty = 2 \times 10^{-10}$ mol cm^{-2}, and $a = 10^{-6}$ mol cm^{-3}. The surface activity coefficient represents the concentration at which half the interfacial saturation adsorption ($\Gamma = \Gamma_\infty/2$) has been reached: $a = c_\infty/2$. Since the saturation adsorption Γ_∞ corresponds to the saturation bulk concentration c_∞ of a surface-active substance above which $d\gamma_{AW}/dc \approx 0$, after the inflection point (indicated by the arrow in Fig. 7a) the $\gamma_{A/W}(c)$ plot becomes quasi-horizontal. From Figure 7a, one obtains a = 0.00725 vol. %, which is a measure of the surface activity of any surfactant present in the aqueous phase. The data from Figure 7a can be also presented vs. the logarithm of the surfactant concentration $\gamma_{A/W}$–ln c. For such a plot, the slope resulting from the Gibbs adsorption equation $d\gamma_{A/W}/\ln c = RT\Gamma$ in a high concentration regime again indicates saturation adsorption occurring at a value of c greater than 0.0145 vol. %.

Natural water samples contain a complex mixture of surface-active compounds of largely unknown makeup and concentration. However, the average value of the activity coefficient a can be derived from surface tension measurements performed on a natural sea water sample (where c_x – unknown surfactant concentration) and its dilutions in ultrapure distilled water (with concentrations $c_x/n, n = 1, 2, \ldots$ etc.). By way of example, Figure 7b shows the dependence of the sea water surface tension as a function of the relative surface-active substance concentration c_d/c_x where $c_d = c_x/n$ is the concentration in a sea water sample diluted n times, recorded for natural water collected at Orłowo (Gulf of Gdańsk, Baltic Sea) on 4 June 2006. The inflection point (indicated by the arrow) at $c_d/c_x = 0.12$ (± 0.03) corresponds to the instant of saturated adsorption layer formation ($\Gamma_\infty \sim c_{d\infty}$). Thus, Szyszkowski's relative activity coefficient is equal to $a_r = c_{d\infty}/2 = 0.12c_x/2 = 0.06c_x$. Such an approach yields a universal measure of sea water sample surface activity referred to the concentration of the original sample c_x. Field measurements of surface tension made on several sea water samples collected in the shallow coastal waters of the Baltic Sea (Gulf of Gdańsk) enabled mean values of a_r ranging from 0.05 c_x to 0.48 c_x to be established. Equilibrium values of γ_{AW} from

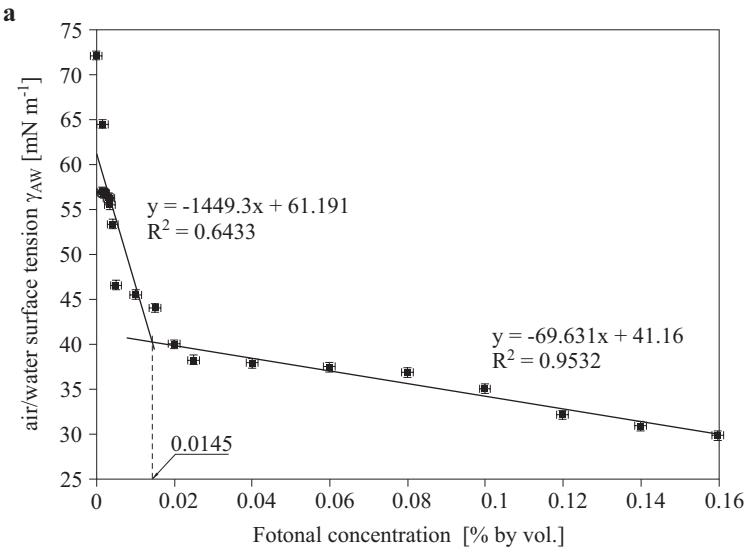

Fig. 7a. Surface tension of the aqueous phase versus concentration (% by vol.) of wetting agent (Fotonal). The arrow indicates the saturation concentration c_∞ corresponding to the formation of the saturated adsorbed layer

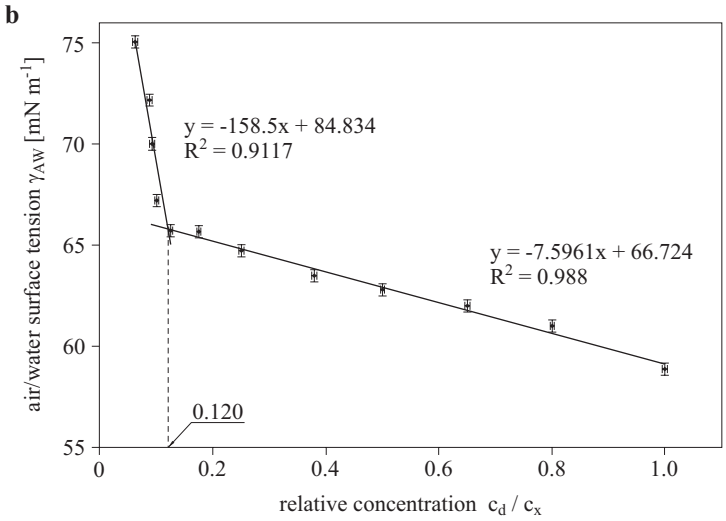

Fig. 7b. Surface tension of a natural sea water sample (collected at Orłowo, Gulf of Gdańsk, Baltic Sea, on 4 June 2006) as a function of the relative surface-active substance concentration c_d/c_x. The arrow indicates the critical value $c_{d\infty}/c_x = 0.12$ corresponding to Szyszkowski's relative surface activity coefficient $a_r = 0.06\ c_x$. The straight line best-fit approximations to the data were used to determine the inflection point

42.94 to 65.55 mN m^{-1} (for pH 7.0–7.8), recorded in several coastal waters of the Baltic Sea (the locations of the sampling stations are shown in Fig. 1 in Pogorzelski & Kogut (2003)), exhibited spatial and temporal variability (see Fig. 8); they are generally lower than the reference value for artificial sea water (dashed line).

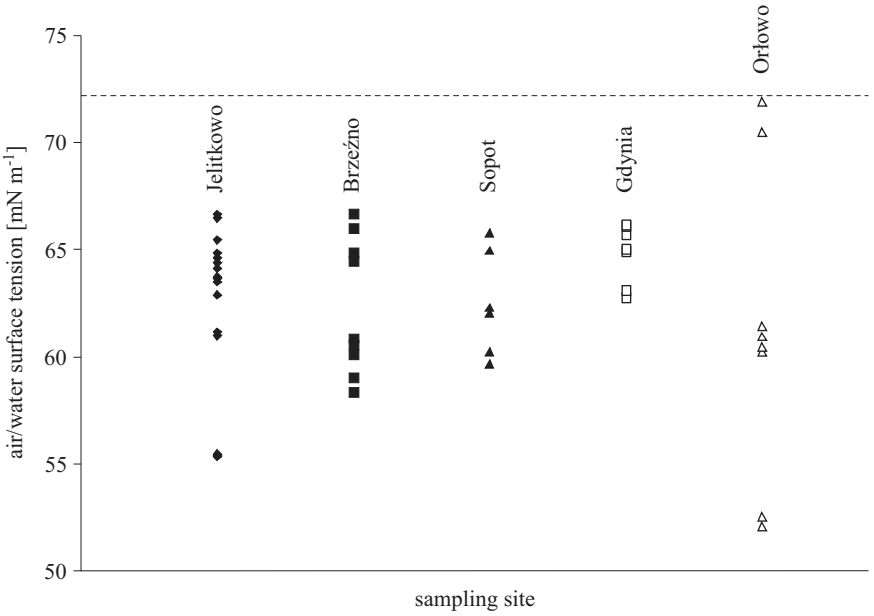

Fig. 8. Spatial and temporal variability of γ_{AW} measured at several marine coastal water stations in April-May 2007 (Gulf of Gdańsk, Baltic Sea). The dashed line corresponds to γ_{AW} value for artificial sea water

Temperature had a significant effect on interfacial tension. The decrease in γ_{AW} of the aqueous phase with increasing temperature can be attributed to the temperature dependence of γ_{AW} for pure water (Lide (ed.) 2003). For an oil/water interface, γ_{OW} was found to increase with growing temperature, demonstrating a negative excess entropy effect of such an interface as evidenced for sunflower oil/water and soybean oil/water systems (Krog 1991, Gaonkar 1992). Finally, γ_{OA} was found to decrease with increasing temperature, as reported in the literature for γ_{OA} of pure triglycerides (Chumpitaz et al. 1999) and a variety of vegetable oils (Flingoh & Let 1992). Because of the temperature dependence of γ_{OW} and γ_{OA}, the minimum threshold value γ_{AW} (allowing spreading, i.e. $S = 0$) shifts to higher values with rising temperature. The spreading coefficient was found to increase asymptotically towards zero with increasing temperature and with a decreasing number of carbon atoms in the hydrocarbon molecule

chain for n-aliphatic hydrocarbons on water (Takii & Mori 1993, Akatsuka et al. 1995). The dynamics of oil lens spreading on a substrate liquid (to be considered in further studies) is a complicated fluid mechanical process also dependent on S. For pure liquid-on-liquid spreading, a thin precursor film (often referred to as a monolayer) extends beyond the main body of the lens, driven by surface tension gradients. The spreading radius of such precursor films depends on the initial spreading coefficient and on the supporting fluid viscosity and density, but not on the lens viscosity. When the substrate liquid is deep, the transient precursor film radius $\mathrm{r_L(t)}$ obeys a simple 3/4 power scaling law with respect to time elapsed t (Svitova et al. 1999):

$$\mathrm{r_L(t)} = \mathrm{K}\left[\frac{S^{1/2}}{(\mu\rho)^{1/4}}\right]\mathrm{t}^{3/4}, \tag{9}$$

where μ and ρ are the viscosity and density of the substrate liquid, respectively, and K is an experimental constant that can vary between 0.665 and 1.52. Chauchan et al. (2000) argue that eq. (9) is valid for the expansion rate of a drop with surfactants present, provided that Marangoni forces drive the spreading, and that the surface tension gradients causing the spreading scale as the initial spreading coefficient divided by the radius of the droplet $\mathrm{r_L}$, i.e. $\mathrm{d}(\gamma_{\mathrm{OA}} + \gamma_{\mathrm{OW}})/\mathrm{dr} = S/\mathrm{r_L}$, where r is the radial position in cylindrical coordinates measured from the drop centre. In another study on the modelling of oil spill evolution, spreading is determined by the rate of area growth, apparently dependent on S given in the form (Sebastião & Guedes Soares 2006):

$$\frac{\mathrm{dA}}{\mathrm{dt}} = \mathrm{K_1 A^{1/3}}\left[\frac{\mathrm{V}}{\mathrm{A}}\right]^{4/3}, \tag{10}$$

where A is the spill area [$\mathrm{m^2}$], $\mathrm{K_1}$ the constant default value (= 150 $\mathrm{s^{-1}}$), V the spilled volume [$\mathrm{m^3}$] and t the time elapsed [s]. The surface properties of natural water bodies and the inherent spreading signatures of different crude-oil derivatives on water obtained under laboratory conditions by means of an optical system, to be adopted as a buoy-like arrangement in studies at sea, represent key input data needed for modelling the kinetics of oil spill spreading.

5. Conclusions

Equilibrium and inherent spreading signatures of oils with different properties were determined in natural sea, artificial sea and distilled waters by means of an optical method for assessing the location, extent and thickness of an oil pollutant. The variability in surface properties of natural sea water due to the presence of microlayer surfactants, as expressed by

γ_{AW} and Szyszkowski's relative coefficient of surface activity a_r, play a key role in modelling the surface-tension-gradient-driven spreading of oil at sea. The spreading parameters obtained in our studies represent the principal input data required in the modelling of the spatial and temporal evolution of oil spills.

The wettability parameters E and S take values similar to those characteristic of long-chain aliphatic hydrocarbons spreading on pure water. From direct photographic measurements, important relations of the normalized relative lens radius r_L/r_{drop} and spreading coefficient S versus the water surface tension γ_{AW} were determined, as they are of significant value in oil spill assessment studies at sea. The spreading coefficients derived by an optical method based on measurements of the equilibrium thickness of sufficiently large lenses ($r_L > 5$–17 cm) are in excellent agreement with those computed from direct surface and interfacial tension measurements (stalagmometric and Wilhelmy plate methods); the equation $S \sim t_\infty^2$ is no longer valid for small oil spots ($r_L < 1$–2 cm). A systematic trend between spreading coefficients and hydrocarbon density was found (as $S \uparrow$ with $\rho_O \downarrow$); this corresponds well with the variability of surface tension with density observed for long-chain paraffin hydrocarbons. For oil lenses of radii several times larger than the water capillary length $r_L >> L_C$, where lens edge interfacial forces can be neglected in comparison to gravity, S can be obtained from the equilibrium thickness t_∞ of the lens with very good accuracy. A difficult problem remaining to be solved in oil pollution assessment techniques is to quantify the geometry, in relation to environmental factors, of an oil spillage in the form of small dispersed spots (radii $\sim$ 1–2 cm); this is currently not predictable on the basis of existing theoretical models of the mutual wettability of liquids. A promising approach based on a novel optical method (applicable following slight modifications to the field study methodology) with empirical relations for selected hydrocarbon-sea water systems is presented here. The effect of temperature and lens aging on the spreading characteristics of crude oil derivatives with different physicochemical properties remains to be quantified in further laboratory and field studies.

References

Adamson, A. W., Gast A. P., 1997, *Physical chemistry of surfaces*, John Wiley and Sons, NY, 808 pp.

Akatsuka S-Y., Yoshigiwa H., Mori Y. H., 1995, *Temperature dependencies of spreading coefficients of hydrocarbons on water*, J. Colloid Interf. Sci., 172 (2), 335–340.

Aveyard R., Clint J. H., 1997, *Liquid lenses at fluid/fluid interfaces*, J. Chem. Soc. Faraday T., 93 (7), 1397–1403.

Bauget F., Langevin D., Lenormand R., 2001, *Dynamic surface properties of asphaltenes and resins at the oil–water interface*, J. Colloid Interf. Sci., 239 (2), 501–508.

Bergeron V., Fagan M. E., Radke C. J., 1993, *Generalized entering coefficients: a criterion for foam stability against oil in porous media,* Langmuir, 9 (7), 1704 –1713.

Camp D. W., Berg, J. C., 1987, *The spreading of oil on water in the surface tension regime*, J. Fluid Mech., 184, 445–462.

Chauhan A., Svitova T. F., Radke C. J., 2000, *A sorption-kinetic model for surfactant-driven spreading of aqueous drops on insoluble liquid substrates*, J. Colloid Interf. Sci., 222 (2), 221–232.

Chumpitaz L. D. A., Coutinho L. F., Meirelles A. J. A., 1999, *Surface tension of fatty acids and triglycerides*, J. Am. Oil Chem. Soc., 76 (3), 379–382.

Clark C. D., 1993, *Satellite remote sensing of marine pollution*, Int. J. Remote Sens., 14 (16), 2985–3004.

Craster R. V., Matar O. K., 2006, *On the dynamics of liquid lenses*, J. Colloid Interf. Sci., 303 (2), 503–516.

Flingoh C. H., Let C. C., 1992, *Surface tensions of palm oil, palm olein and palm stearin,* Elaeis, 4 (1), 27–31.

Gaonkar A. G., 1992, *Effects of salt, temperature and surfactants on the interfacial tension behavior of a vegetable oil/water system,* J. Colloid Interf. Sci., 149 (1), 256–260.

Harkins W. D., Feldman A., 1922, *Films. The spreading of liquids and the spreading coefficient*, J. Am. Chem. Soc., 44, 2665–2685.

Hotrum N. E., Cohen Stuart M. A., van Vliet T., Avino S. F., van Aken G. A., 2002, *Monitoring entering and spreading of emulsion droplets at an expanding air/water interface: a novel technique*, J. Colloid Interf. Sci., 247 (1), 125–131.

Hotrum N. E., Cohen Stuart M. A., van Vliet T., Avino S. F., van Aken G. A., 2003, *Entering and spreading of protein stabilised emulsion droplets at the expanding air/water interface*, [in:] *Food colloids, biopolymers and materials*, E. Dickinson & T. van Vliet (eds.), Roy. Soc. Chem., Cambridge, 192–199.

Hotrum N. E., Cohen Stuart M. A., van Vliet T., Avino S. F., van Aken G. A., 2003, *Flow and fracture phenomena in adsorbed protein layers at the air/water interface in connection with spreading oil droplets*, Langmuir, 19 (24), 10210 –10216.

Hotrum N. E., Cohen Stuart M. A., van Vliet T., Avino S. F., van Aken G. A., 2004, *Spreading of partially crystallized oil droplets on an air/water interface*, Colloid. Surface. A, 240 (1), 83–92.

Hotrum N. E., Cohen Stuart M. A., van Vliet T., Avino S. F., van Aken G. A., 2005, *Elucidating the relationship between the spreading coefficient, surface-mediated partial coalescence and the whipping time of artificial cream*, Colloid. Surface. A, 260 (1–3), 71–78.

Hunter K. A., Liss P. S., 1981, *Organic sea surface films*, [in:] *Marine organic chemistry*, E. K. Duursma & R. Dawson (eds.), Elsevier, New York, 259–298.

Kaniewski E., 1974, *Influence of sea surface oil contamination on gas exchange and light transmission*, Ph. D. thesis, Geophys. Inst. PAS, Warsaw, (in Polish).

Krog N. J., 1991, *Thermodynamics of interfacial films in food emulsions*, [in:] *Microemulsions and emulsions in foods*, M. A. El-Nokaly & D. Cornell (eds.), Am. Chem. Soc., Washington, DC, 138–145.

Law B. M., 2001, *Wetting, adsorption and surface critical phenomena*, Prog. Surf. Sci., 66 (6), 159–216.

Lide D. R. (ed.), 2003, *CRC handbook of chemistry and physics*, 84th edn., CRC Press, Boca Raton, FL, 2300 pp.

Lobo L., Wasan D. T., 1993, *Mechanisms of aqueous foam stability in the presence of emulsified non-aqueous-phase liquids: structure and stability of the pseudoemulsion film*, Langmuir, 9 (7), 1668–1677.

Pogorzelski S. J., Kogut A. D., 2003, *Structural and thermodynamic signatures of marine microlayer surfactant films*, J. Sea Res., 49 (4), 347–356.

Pujado P. R., Scriven L. E., 1972, *Sessile lenticular configurations: translationally and rotationally symmetric lenses*, J. Colloid Interf. Sci., 40 (1), 82–98.

Retter U., Vollhardt D., 1993, *Formation of lenticular nuclei from an insoluble monolayer at the air/water interface: a model*, Langmuir, 9 (9), 2478–2480.

Robinson J. V., Woods W. W., 1948, *A method of selecting foam inhibitors*, J. Soc. Chem. Ind. Lond., 67, 361–365.

Schokker E. P., Bos M. A., Kuijpers A. J., Wijnen M. E. Walstra P., 2002, *Spreading of oil from protein stabilized emulsions at air/water interfaces*, Colloid. Surface. B, 26 (4), 315–327.

Sebastião P., Guedes Soares C., 2006, *Uncertainty in predictions of oil spill trajectories in a coastal zone*, J. Marine Syst., 63 (3–4), 257–269.

Svitova T. F., Hill R. M., Radke C. J., 1999, *Spreading of aqueous dimethyldidodecylammonium bromide surfactant droplets over liquid hydrocarbon substrates*, Langmuir, 15 (21), 7392–7402.

Takii T., Mori Y. H., 1993, *Spreading coefficients of aliphatic hydrocarbons on water*, J. Colloid Interf. Sci., 161 (1), 31–37.